Cellulose (2025) 32:6673–6693
https://doi.org/10.1007/s10570-025-06634-4

ORIGINAL RESEARCH

Understanding interactions of pharmaceutical pollutants with cellulosic materials

Maija Vuoriluoto · Tekla Tammelin · Hannes Orelma

Received: 29 November 2024 / Accepted: 7 June 2025 / Published online: 25 June 2025
© The Author(s) 2025

Abstract This research examines the interaction mechanisms of pharmaceutical pollutants ibuprofen (IBP) and naproxen (NPR) (anti-inflammatory compounds), and 17α-ethinyl estradiol (EE2) (estrogenic compound) with cellulosic materials via adsorption studies utilizing Surface Plasmon Resonance (SPR) technique. The goal was to identify the key factors affecting the affinity between cellulose materials and pollutants in a systematic fashion with real-time adsorption monitoring to support the development of sustainable water purification technologies. The anti-inflammatory and estrogenic compounds were adsorbed on ultrathin films (thickness ~ 10-20 nm) of nanocellulose with varying surface charge (mechanically disintegrated cellulose nanofibrils (CNF) and TEMPO-oxidized cellulose nanofibers (TCNF)), and polymeric cellulose with varying degree of hydrophobicity (regenerated cellulose (RC), cellulose triacetate (CTA) and trimethylsilyl cellulose (TMSC)). Highly hygroscopic and negatively charged nanocellulose surfaces showed low affinity for drugs, while regenerated cellulose exhibited higher adsorption capacity probably due to its amphiphilic nature. Indeed, the hydrophobic character of cellulose derivatives was found to significantly impact pharmaceutical adsorption, especially in case of EE2. Hydrophobic TMSC and CTA films demonstrated adsorption for hormonal pollutant, with nearly ten-fold higher adsorption than anti-inflammatory compounds. Pharmaceuticals were detectable on hydrophobized cellulose surfaces at trace concentrations of 0.1–1 µg/mL. Langmuir adsorption model showed the highest adsorption coefficient for EE2 on TMSC, emphasizing its efficacy at capturing hormonal pollutants at low concentrations. Adsorption was mostly irreversible after rinsing, highlighting the need for specific modifications to cellulose to achieve desired selectivity and efficiency for pollutant removal. These findings aid in designing efficient membrane and sensor systems for capturing and purifying pharmaceutical-contaminated water streams.

Keywords Pharmaceutical pollutants · Interaction · Surface analytics · SPR · Ultrathin films · Nanocellulose · Regenerated cellulose · Cellulose derivatives · Hydrophobization

Introduction

With declining water resources, novel, and sustainable alternatives are required for more efficient wastewater treatment to battle against persistent and harmful emerging micropollutants with lower cost

Supplementary Information The online version contains supplementary material available at https://doi.org/10.1007/s10570-025-06634-4.

M. Vuoriluoto (✉) · T. Tammelin · H. Orelma
VTT Technical Research Centre of Finland Ltd., Tietotie 4E, P.O. Box 1000, FI-02044 Espoo, Finland
e-mail: maija.vuoriluoto@vtt.fi

and lesser energy demand (Samanta et al. 2019). Pharmaceutical pollutants or micropollutants refer to residues or traces of pharmaceutical compounds that enter the environment through various routes, such as improper disposal, excretion by humans and animals, and wastewater from pharmaceutical manufacturing facilities (Mansouri et al. 2021; Eniola et al. 2022; Chakraborty et al. 2023). Severe adverse effects of pharmaceutical micropollutants, such as anti-inflammatory drugs or estrogen hormones, include organism estrogenicity, mutagenicity, and genotoxicity (Das 2017; Chakraborty et al. 2023) and bio-accumulation via adhesion to nano- and microplastics (Li et al. 2018; Mansouri et al. 2021). In addition, pharmaceutical residues pose adverse effects on aquatic ecosystems, cause human health concerns, e.g., antibiotic resistance, are designed to be biologically active and resistant to degradation, and can incur significant economic costs for water treatment facilities, agriculture, and ecosystem restoration efforts. Micropollutants accumulated in aquatic systems, soil, and air are cause for major global concern due to the incapability of conventional membrane processes to sufficiently remove, eliminate, or biotransform most of these substances (Das 2017; Poerio et al. 2019).

Current removal methods for pharmaceutical micropollutants include physical, chemical, and biological methods. Membrane filtration techniques and adsorption processes belong to physical methods whereas chemical methods include coagulation, oxidation, irradiation, and advanced oxidation processes (AOPs) (Loganathan et al. 2023). The activated carbon adsorption process is highly effective in removing a wide range of pharmaceutical compounds due to its large surface area and high adsorption capacity but with limited removal efficiency for certain types of pharmaceuticals. Moreover, it requires frequent regeneration or replacement of the activated carbon (Rivera-Utrilla et al. 2011; Wong et al. 2018). Microbial degradation and microbial biomass adsorption as well as membrane bioreactors fall to biological methods (Taoufik et al. 2021). In the advanced oxidation process pharmaceutical pollutants are degraded leading to the formation of non-toxic byproducts. However, AOP is energy-intensive and expensive and may result in harmful byproducts and secondary equally disruptive pollutants (Ganiyu et al. 2022). Membrane filtration techniques such as reverse osmosis (RO) and nanofiltration (NF), despite high energy demand and fouling issues, effectively remove pharmaceuticals through physical separation based on size and molecular weight as well as physicochemical properties (Hube et al. 2020; Loganathan et al. 2023). Biological treatment methods e.g., activated sludge and biofiltration degrade pharmaceuticals cost-effectively and environmentally sustainably through microbial metabolism but is limited to certain pharmaceuticals, is susceptible to fluctuations in composition, and long retention times (Loganathan et al. 2023).

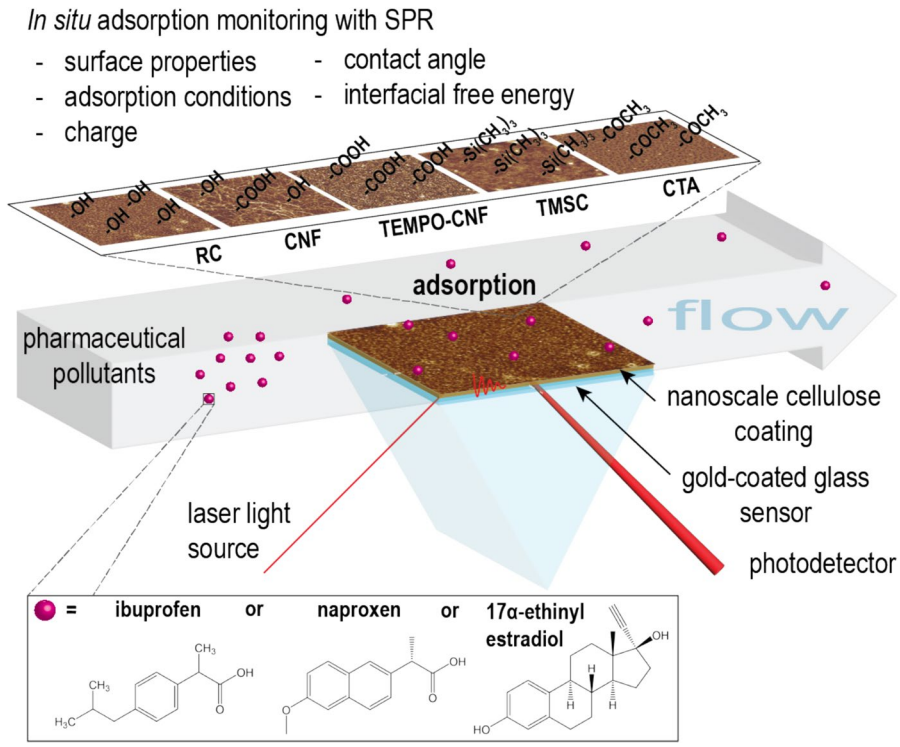
Addressing pharmaceutical pollution requires a multifaceted approach where most promising solutions to achieve effective water treatment in the future will combine multiple processing techniques (Eniola et al. 2022). Membrane filtration techniques and membrane bioreactors (MBRs) have demonstrated most promise for efficient removal of micropollutants and microplastics (Yang et al. 2019; Poerio et al. 2019; Song et al. 2020). Cellulose-based solutions have potential to complement existing treatment methods and contribute to more efficient and eco-friendly wastewater treatment practices (Mautner 2020). Cellulose-based (nano)materials exhibit promise as membrane materials due to their abundance including waste and side-stream materials, sustainable origin and unique properties (e.g., large surface area), film-forming tendency, hydrophilicity, and potential for functionalization (Liu et al. 2010; Junter and Lebrun 2017; Vuoriluoto et al. 2017; Orelma et al. 2018, 2020; Thomas et al. 2018; Trache et al. 2020; Das et al. 2022; Qi et al. 2023; Goswami et al. 2024). Additionally, cellulose materials do not introduce additional harmful chemicals or byproducts into the environment. Nanocellulose materials, such as cellulose nanofibrils (CNF) and cellulose nanocrystals (CNC), have already shown potential for pressure-driven filtration systems and for thin nanocellulose coatings as functional barrier layers for filtration membranes (Ma et al. 2010, 2014; Chen et al. 2019, 2021; Pöhler et al. 2022; Sharma et al. 2022). Nanocellulosic materials remove cations very effectively, such as heavy metal ions, as well as dyes, pesticides, and pharmaceuticals mostly via electrostatic interactions or through appropriate modification (Mohammed et al. 2018; Mautner 2020; Ahankari et al. 2020). Regenerated cellulose (RC) commercial membranes have been utilized for decades in separation techniques, for example ultrafiltration (UF, pore size 2–100 nm), however, non-biodegradable cellulose

acetate membranes are more common in NF (pore size 1–2 nm) and RO (pore size 0.1–1 nm) because of environmental concerns associated with traditional cellulose solvents (Livazovic et al. 2015; Yang et al. 2019).

Due to the many advantageous qualities of cellulose-based materials, they have been demonstrated as potential purification materials for pharmaceutical pollutants. Cellulose nanofibrils and cellulose nanocrystals are emerging as effective adsorbent materials for pharmaceutical residues (Siqueira et al. 2010). Cellulosic composite materials with e.g., graphene oxide, carbon nanotubes (Durairaj et al. 2019, 2022; Zhang et al. 2023) or metal oxides (Iqbal et al. 2022) have been observed to enhance the removal efficiency of wastewater pollutants. Increased affinity of hormonal estrogen on nanocellulose has been achieved with modification utilizing cyclodextrins containing hydrophobic cavities (Orelma et al. 2018). Regeneration and reusability of cellulosic adsorbents have also been investigated to e.g. improve sustainability and cost-effectiveness (Ge et al. 2016; Gupta et al. 2023). Furthermore, cellulosic materials offer advantageous properties to filtration systems through size exclusion and adsorption mechanisms as well as high porosity, mechanical strength, and chemical stability (Mautner 2020). Nanocellulosic materials are also hygroscopic (Solhi et al. 2023) and exhibit antifouling properties (Hakalahti et al. 2015; Aguilar-Sanchez et al. 2021; Pöhler et al. 2022).

Understanding interfacial interactions between cellulosic materials and pharmaceutical residues (anti-inflammatories and estrogenic compounds) will facilitate development of novel strategies for sustainable water purification technologies with potential for controlled affinity and selective capture and degradation of the pollutants much needed due to health impacts and diminishing freshwater resources in the world. The objective in this work was to observe in real-time the adsorption behavior of pharmaceuticals on cellulosic materials to understand the interactions and how to influence them at a fundamental level to assess potential routes to develop high-efficiency wastewater treatment methods, which is not typically feasible with more traditional adsorption studies. Cellulosic ultrathin films (thickness ~ 10–20 nm) (Ahola et al. 2008b; Kontturi et al. 2011; Hakalahti et al. 2017) enable monitoring of adsorption behavior and interactions in situ with Surface Plasmon Resonance (SPR) technique. Surface hydrophobization of cellulosic materials could have potential as a simple technique to increase capture of pharmaceutical residues from contaminated water sources to contribute to the development of more sustainable alternatives for synthetic adsorbent materials. The aim here was to increase the fundamental understanding of cellulose (nano)material interfacial interactions with pharmaceutical pollutants and investigate the effect of modifying e.g., the surface hydrophobicity of the cellulosic substrates (Scheme 1). The information gained could have a significant impact on the selection of appropriate cellulosic materials or modification routes in future investigations developing and designing high-performance water treatment membranes.

Nonsteroidal anti-inflammatory drugs, such as ibuprofen and naproxen, were selected as model pharmaceuticals due to their widespread consumption and occurrence as e.g., only 15–23% ibuprofen is adsorbed via ingestion while the rest end up in water systems (Khadir et al. 2020). Other problematic pharmaceuticals are estrogenic compounds, as the removal efficiency for these highly persistent and biologically active (Schäfer et al. 2002) compounds at wastewater treatment plants varies greatly with concentrations as high as 2.6 µg/L reported in the US for 17α-ethinyl estradiol (EE2), the main component of the contraceptive pill (Nghiem et al. 2004), therefore, selected as model estrogen. The adsorption mechanisms of ibuprofen, naproxen and 17α-ethinyl estradiol with cellulose nanofibril (fibrillar cellulose with a residual xylan hemicellulose and moderate charge), TEMPO-oxidized cellulose nanofibril (highly charged anionic fibrillar cellulose) and regenerated cellulose (pure polymeric cellulose with low charge) ultrathin films were investigated in situ with SPR and Atomic Force Microscopy (AFM). The real-time measurements allow for careful monitoring and observation of the adsorption process and facilitate the evaluation of e.g. rinsing on the adsorption that can reveal novel insight into the interaction mechanisms of materials. The effect of surface hydrophobicity on pharmaceutical adsorption was investigated by applying trimethylsilyl cellulose (TMSC) and cellulose triacetate (CTA) ultrathin films. Contact angle (CA) measurements were performed to investigate the influence of surface energy on interactions. Influence of pH and adsorbate concentration on adsorption behavior was also investigated with SPR and acquired data was



Scheme 1 Schematic representation of pharmaceutical pollutant adsorption studies with cellulosic ultrathin films, fibrillar nanocellulose with moderate (CNF) and high charge (TEMPO-CNF), low charged polymeric pure regenerated cellulose (RC), polymeric hydrophobized cellulose (TMSC, CTA), investigated in situ with Surface Plasmon Resonance (SPR). Included also structures of studied pharmaceuticals ibuprofen (IBP), naproxen (NPR) and 17α-ethinyl estradiol (EE2)

fitted to the Langmuir adsorption model. The objective was to increase understanding of factors, especially surface hydrophobicity, influencing interfacial interactions between pharmaceutical pollutants and cellulose materials to aid in the development of sustainable high-efficiency filtration membrane matrices with maximized and/or controlled affinity toward target compounds selectively to further the goal of providing clean water for all.

Experimental

Materials

Nanocellulose materials

Two grades of cellulose nanofibrils i.e., mechanically disintegrated native CNF (Tenhunen et al. 2014) and 2,2,6,6-tetramethyl-1-piperidinyloxyl (TEMPO) oxidized CNF (Saito et al. 2006) were utilized. Never-dried bleached kraft pulp with residual xylan obtained from a Finnish pulp mill was used to prepare native CNF though mechanical disintegration. First, the pulp was soaked at 1.7wt% consistency followed by dispersion utilizing a high-shear Diaf dissolver (Minibatch Type20) for 10 min at 700 rpm. A Masuko grinder (Supermasscolloider MKZA10-151, Masuko Sangyo Co., Japan) at 1500 rpm was used to pre-refine the pulp suspension which was followed by fluidization to nanofibers by six passes through a Microfluidics M-7115–30 microfluidizer (Microfluidics Corp.). The resultant mechanically disintegrated CNF (~ 10 – 100 nm in width and 0.5 – 10 µm in length) had a solid content of ~ 1.6% and anionic charge of 0.04 mmol/g (SCAN-CM 65:2002; Tenhunen et al. 2014) originating from the residual xylan.

TEMPO-mediated oxidation of bleached softwood kraft pulp fibers was performed with a solution of 0.1 mmol TEMPO (Sigma-Aldrich, Finland), 1 mmol NaBr, and 5.00 mmol NaClO in water at pH 10.5 according to Saito et al. (2006). The reaction was ended with ethanol and washed with MilliQ-water. The resultant oxidized fibers were passed twice through a MF7125-30 microfluidizer (Microfluidics Corp.) to yield TEMPO-oxidized cellulose nanofibrils (TCNF, 4 – 20 nm in width and 0.5—2 µm in length). The resultant TCNF had a solid content of ~ 1% and the degree of oxidation per anhydroglucose unit was

1.3 mmol/g. (SCAN-CM 65:2002; Leppänen et al. 2022).

Pure polymeric regenerated cellulose and hydrophobized cellulose materials

Trimethylsilyl cellulose (TMSC) with a DS of ~ 2.1–2.3 (Tammelin et al. 2006) was synthesized by hexamethyldisilazane silylation of microcrystalline cellulose powder from spruce fibers dissolved in DMAc-LiCl as first suggested by Greber and Paschinger (1981) and Cooper et al. (1981). TMSC was regenerated back to pure cellulose by desilylation with hydro-chloric acid vapor treatment (Schaub et al. 1993) producing regenerated cellulose (RC) with low charge (Kontturi et al. 2008). Cellulose triacetate (CTA, acetyl content 44%, DS ~ 2.9, #177822500) was obtained from Thermo Scientific Chemicals.

Pharmaceuticals

Naproxen (NPR, #N8280), ibuprofen (IBP, #I4883) and 17α-ethinyl estradiol (EE2, #E4876) were purchased from Sigma-Aldrich (Helsinki, Finland). The pKa values reported for the pharmaceuticals are 4.15 (p. PubChem Compound Summary for CID 156391, Naproxen.) for NPR, ~ 5 (p. PubChem Compound Summary for CID 3672, Ibuprofen.) for IBP and for EE2 10.46 (Hurwitz and Liu 1977). Their octanol–water partition coefficients (log K_{ow}) are 3.97 (p. PubChem Compound Summary for CID 3672, Ibuprofen.) for IBP, 3.18 (p. PubChem Compound Summary for CID 156391, Naproxen.) for NPR, and 3.67 (p. PubChem Compound Summary for CID 5991, Ethinyl Estradiol.) for EE2. Dimension reported for IBP are 1.03 nm (lenght), 0.52 nm (width) and 0.43 nm (thickness) (Mestre et al. 2007) and for NPR ~ 1.41 nm (length) and ~ 0.74 nm (width) (Wiącek and Przykaza 2022). All used laboratory chemicals were of analytical grade. Deionized water further purified with a Millipore Synergy UV unit (Milli-Q) was used in all experiments.

Methods

Preparation of cellulosic ultrathin films

Spin-coating was applied to produce ultrathin films of CNF, TCNF, RC, TMSC, and CTA and used to study interactions with pharmaceutical molecules. CNF and TCNF are fibrillar nanocellulosic materials whereas RC, TMSC, and CTA are polymeric cellulosic materials. Regenerated cellulose films function as a pure low charged cellulosic reference material for fibrillar charged CNF and TCNF surfaces. Additionally, RC also functions as a polymeric pure cellulose reference material for hydrophobized cellulose material trimethylsilyl cellulose and cellulose triacetate. RC films are also representative of regenerated cellulose films utilized in various established applications. CNF ultrathin films (thickness ~ 10 nm (Ahola et al. 2008b)) were prepared according to Ahola et al. (2008a). TCNF thin films (thickness ~ 10–15 nm (Hakalahti et al. 2017)) were prepared according to Hakalahti et al. (2017) with the slightly modified procedure described by Eronen et al. (2012). In short, CNF- or TCNF-gel was diluted (0.190 wt-% nanocellulose in water) and sonicated using Sonifier® SFX550 Cell Disruptor/Homogenizer (Branson Ultrasonics Corp., Danbury, CT, USA) with a 1/8″ tapered microtip at 25% amplitude for 10 min or 2 min, respectively. The CNF-gel was consecutively centrifuged at 10,400 rpm for 45 min and individual cellulose nanofibrils were obtained from the resultant clear supernatant. The obtained CNF and TCNF were spin-coated (Model WS 400B2, Laurell Technologies, PA, USA) onto UV/ozonized gold SPR (Oy BioNavis Ltd., Ylöjärvi, Finland) or silicon dioxide substrates with a pre-adsorbed thin anchor layer of PEI (3000 rpm, 90 s spinning time). After spin-coating, the CNF and TCNF films were dried at 80 °C for 10 min and stored in a desiccator.

TMSC solution of 10 g/L in toluene or CTA solution of 5 g/L in chloroform was spin-coated at 4000 rpm for 60 s onto Au SPR (Oy BioNavis Ltd., Ylöjärvi, Finland) sensors or silicon dioxide substrates (Kontturi et al. 2003). After deposition, the TMSC and CTA films were annealed at 60 °C for 10 min. Prior to spin-coating, the CTA and TMSC solution were filtered (Pall Acrodisc PTFE, 0.45 µm) to remove any undissolved material. The TMSC surfaces were hydrolyzed to pure regenerated cellulose (RC) ultrathin films by a hydrochloric acid vapor treatment (Schaub et al. 1993) with an average thickness of ~ 20 nm (Kontturi et al. 2011). Prior to measurements in SPR (see methods further below) the sensors were allowed to stabilize in water overnight.

Surface plasmon resonance (SPR)

A multi-parametric Surface Plasmon Resonance instrument (MP-SPR Model Navi 210A, Oy BioNavis Ltd., Ylöjärvi, Finland) was utilized to monitor the adsorption of pharmaceuticals onto cellulosic ultrathin surfaces. In SPR some of the energy of the light is coupled with surface plasmon waves traveling along the solid layer and analyzed solution interface which is observed as a sharp attenuation of light reflectivity. Changes occur in the reflected light energy and angles of maximum reflection intensity (Schasfoort and Tudos 2008). The wavelengths and angles of light at which the surface plasmon resonance effect takes place correlate very sensitively with the refractive indices (RI) of the medium in contact with the surface of the SPR sensor (Jung et al. 1998; Campbell and Kim 2007). The thickness of the adsorbed layer, d, and the adsorbed amount per unit area Δm, were determined with Eq. 1 (Jung et al. 1998) and Eq. 2:(Campbell and Kim 2007)

$$d = \frac{l_d}{2} \frac{\Delta_{angle}}{m\left(n_a - n_0\right)} \tag{1}$$

$$\Delta m = d \times \rho \tag{2}$$

where Δ_{angle} is the change in the SPR angle, l_d is a characteristic evanescent electromagnetic field decay length, estimated as 0.37 of the light wavelength (240 nm), m is a sensitivity factor for the sensor obtained after calibration of the SPR (109.94°/RIU), n_0 is the refractive index of the bulk solution (1.334 RIU), n_a is the refractive index of the adsorbed substance and ρ is the packing density of the adsorbed species. Refractive indices and packing densities for ibuprofen, naproxen and 17α-ethinyl estradiol were assumed to be 1.519 and 0.952 g/cm^3 (p. PubChem Compound Summary for CID 3672, Ibuprofen.), 1.609 and 1.2 g/cm^3 (p. PubChem Compound Summary for CID 156391, Naproxen.), and 1.624 and 1.2 g/cm^3 (p. PubChem Compound Summary for CID 5991, Ethinyl Estradiol.), respectively. Each SPR measurement was performed at least twice with a constant flow of 10 µL/min at 20 °C.

Pharmaceutical adsorption on cellulose nanofibril and pure regenerated cellulose ultrathin films

Adsorption of pharmaceuticals ibuprofen, naproxen and 17α-ethinyl estradiol onto CNF, TCNF and RC films was monitored in situ in SPR. First, a stock solution was prepared by dissolving 100 mg of respective pharmaceutical in 10 mL of ethanol due to poor solubility in aqueous media. Then, stock solutions were appropriately diluted to prepare 0.1 mg/mL solutions of respective pharmaceutical in 10 mM phosphate buffer solution (pH 6.8). The prepared 0.1 mg/mL pharmaceutical solutions were then allowed to adsorb on CNF, TCNF and RC surfaces for 60 min followed by buffer rinsing as monitored by SPR. Background phosphate buffer contained 1% ethanol to eliminate impact of the stock solution ethanol on SPR signal.

Pharmaceutical adsorption on hydrophobized cellulose ultrathin films

The effect of surface hydrophobization on pharmaceutical adsorption was studied by performing similar adsorption measurements on TSMC and CTA ultrathin films where 0.1 mg/mL pharmaceutical solutions were allowed to adsorb on respective hydrophobized cellulose surfaces for 60 min followed by buffer (10 mM phosphate buffer, pH 6.8) rinsing as monitored by SPR.

Atomic force microscopy

Bruker MultiMode 8 AFM was utilized to analyze the changes in surface topography of CNF, TCNF, RC, TMSC and CTA ultrathin films upon pharmaceutical adsorption. SiO_2 disks (1×1 cm^2) with spin-coated cellulosic material (as described above) were immersed in a petri dish for 30 min followed by immersion in 0.1 mg/mL solution of IBP, NPR or EE2 for 60 min. After rinsing films were dried with nitrogen gas and stored in a desiccator prior to imaging with AFM. Tapping mode in air with silicon cantilevers (HQ:NSC15/Al BS, MikroMasch, Innovative Solutions Bulgaria Ltd.) was applied to scan surface areas of 5×5 µm^2. At least three separate areas on each sample were imaged with flattening being the only image processing step applied.

Effect of concentration on pharmaceutical adsorption

Pharmaceuticals were consecutively adsorbed on RC, TMSC and CTA surfaces at different concentrations of 0.1 µg/mL, 1 µg/mL, 10 µg/mL and 100 µg/mL (10 mM phosphate buffer at pH 6.8) for 30 min each, followed by buffer rinsing to investigate effect of pharmaceutical concentration on adsorption. To further investigate the mechanism of pharmaceutical adsorption onto cellulosic surfaces, the adsorption data were fitted to Langmuir adsorption isotherm Eq. 3:

$$q_e = \frac{Q_m K_L c_e}{1 + K_L c_e} \tag{3}$$

where q_e is adsorbed amount (mg/m^2), Q_m is maximum adsorption capacity (mg/m^2), K_L is adsorption coefficient and c_e is adsorbate concentration (µg/mL).

Contact angle measurements and surface energy

Contact angle (CA) measurements were utilized to assess surface energy (SE), its components, and the interfacial free energy of spin-coated CNF, TCNF, RC, TMSC and CTA ultrathin films on SiO_2 with four probing liquids with various surface tensions (ethylene glycol, water, diiodomethane, and formamide). An Attention Theta Optical Tensiometer (Biolin Scientific Ab, Sweden) was utilized for CA measurements of sessile drops on the cellulosic films. Three to five measurements per sample were used to present an average value for results and the experiments were performed at 23 °C and 50% relative humidity (RH).

Using CA data and Young's equation, the solid/liquid interfacial energy was calculated with Eq. 4:

$$\frac{(1+\cos\theta)\gamma_l}{2} = \sqrt{\gamma_s^d \gamma_l^d} + \sqrt{\gamma_s^- \gamma_l^+} + \sqrt{\gamma_s^+ \gamma_l^-} \tag{4}$$

The dispersive ($\gamma_s^{\,d}$) and polar (acid–base) contributions of a solid material are estimated in this method, where the latter is further divided into the electron acceptor or Lewis acid parameter ($\gamma_s^{\,+}$) and the electron donor or Lewis base parameter ($\gamma_s^{\,-}$).

Furthermore, to determine the hydrophilic or hydrophobic nature of the surface the interfacial free energy of the films (ΔG_{sws}^{IFE}) was evaluated (Van Oss et al. 1988). ΔG_{sws}^{IFE} is defined as the energy of interaction between particles or molecules of a solid material (s) immersed in a liquid (water, w):

$$\Delta G_{sws}^{IFE} = -2\gamma_{sw} = -2 \cdot \left(\gamma_{sw}^D + \gamma_{sw}^P\right) \tag{5}$$

The Good–Girifalco–Fowkes rule (Good and Girifalco 1960) gives the relation of the dispersive component (Lifshitz–van der Waals interactions) of interfacial tension to the individual surface tension of the solid material (s) and water (w):

$$\gamma_{sw}^D = \left(\sqrt{\gamma_s^D} - \sqrt{\gamma_w^D}\right)^2 \tag{6}$$

The expression of the polar component of the interfacial tension between s and w is given as:

$$\gamma_{sw}^P = 2 \cdot \left(\sqrt{\gamma_s^+ \gamma_s^-} + \sqrt{\gamma_w^+ \gamma_w^-} - \sqrt{\gamma_s^+ \gamma_w^-} - \sqrt{\gamma_w^+ \gamma_s^-}\right) \tag{7}$$

Regeneration of adsorbed pharmaceuticals from hydrophobized cellulose films

The regeneration of adsorbed pharmaceuticals from the cellulosic surfaces was investigated by applying 99.5% ethanol or sodium dodecyl sulfate solution (SDS, 0.5 wt-% in 10 mM phosphate buffer at pH 6.8, 1% ethanol) on RC, TMSC or CTA surfaces with adsorbed pharmaceutical for 10 min followed by rinsing with respective buffer solution.

Effect of pH on naproxen adsorption

Naproxen with concentration of 0.1 mg/mL was adsorbed on RC surface at pH 4 (10 mm acetate buffer) and pH 9.5 (10 mM carbonate buffer) to study the effect of pH on adsorption behavior. Naproxen was chosen as the model pharmaceutical due to its most ionizable nature making it most susceptible to effects of pH variation, and lowest octanol–water partition coefficient indicating lowest hydrophobicity.

Results and discussion

Pharmaceutical adsorption on cellulose nanofibrils

First, the effect of cellulose charge on the adsorption of pharmaceutical residues was investigated and

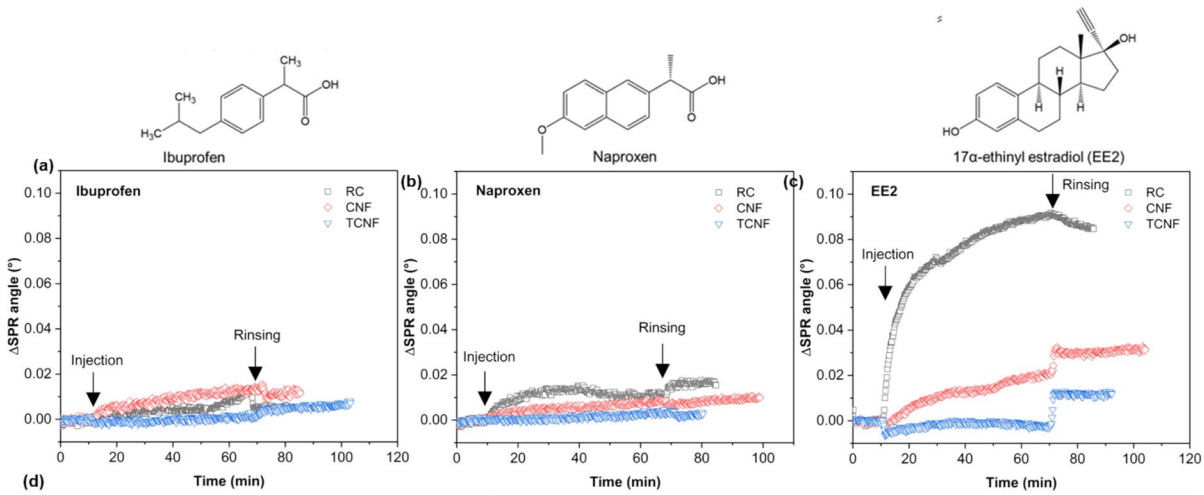
monitored with SPR. Two different nanocelluloses were selected with varying charge density i.e., cellulose nanofibrils with moderate charge of 0.04 mmol/g originating from residual xylan and TEMPO-oxidized cellulose nanofibrils with high charge (1.3 mmol/g) resulting from the COOH-groups introduced during the oxidation process. Regenerated cellulose surfaces, representing pure cellulose with low charge density due to the dissociation of hydroxyl groups, were also investigated as a reference system. Three pharmaceuticals with different pKas and hydrophobicities were selected: ibuprofen, naproxen, and 17α-ethinyl estradiol. IBP and NPR are non-steroidal anti-inflammatory drugs that have a carboxylic acid group that can be ionized depending on the pH (pKa for NPR 4.15 (p. PubChem Compound Summary for CID 156391, Naproxen) and for IBP ~ 5 (p. PubChem Compound Summary for CID 3672, Ibuprofen.)). EE2 is a synthetic estrogen that has a phenolic hydroxyl group that can also be ionized (pKa for EE2 10.46 (Hurwitz and Liu 1977)). The hydrophobicity of the pharmaceuticals quantified by their octanol–water partition coefficients (log K_{ow}) are 3.97 (p. PubChem Compound Summary for CID 3672, Ibuprofen.) for IBP, 3.18 (p. PubChem Compound Summary for CID 156391, Naproxen.) for NPR, and 3.67 (p. PubChem Compound Summary for CID 5991, Ethinyl Estradiol.) for EE2. The respective pharmaceutical (IBP, NPR, EE2) was adsorbed on the cellulosic surface with increasing charge (RC < CNF < TCNF)) at neutral pH for 60 min followed by rinsing as monitored in situ with SPR (Fig. 1).

Based on SPR data all pharmaceutical substances in this work exhibited low affinity towards medium charged CNF and highly charged TCNF at neutral pH (Fig. 1). As expected, the mostly hydrophobic pharmaceuticals showed very low interaction with highly hydrophilic and water swollen TCNF film. For the CNF film all pharmaceuticals indicated low affinity although somewhat higher interaction compared to the TCNF surface. AFM height and phase images also support the conclusion of negligible adsorption of pharmaceuticals on nanocellulose films with no significant changes observed (Figs. S1 and S2, see supporting information). Overall, the results indicated poor adsorption of the pharmaceuticals onto water-swollen hydrophilic anionic nanocellulose surfaces, most likely due to the more hydrophobic nature of the pharmaceuticals, and for IBP and NPR possibly also charge repulsion as their structures exhibit a carboxylic acid group which is deprotonated at neutral pH.

On the low-charged pure cellulose RC surface, ibuprofen and naproxen exhibited similar adsorption as on negatively charged nanocellulose surfaces (Fig. 1a,b). Higher adsorption onto RC (0.32 nm and 0.38 mg/m^2) than on the CNF (0.12 nm and 0.14 mg/m^2) and TCNF surfaces (0.05 nm and 0.06 mg/m^2) was observed for hormone EE2 (Fig. 1c,d), probably due to non-polar interactions with the pure cellulose surface. Even though all tested pharmaceuticals have very limited solubility in aqueous media (LogS for IBP −3.99 (p. PubChem Compound Summary for CID 3672, Ibuprofen.) and for NPR −4.16 (p. PubChem Compound Summary for CID 156391, Naproxen.)), hormone EE2 is the least soluble in water (LogS value −4.3) (p. PubChem Compound Summary for CID 5991, Ethinyl Estradiol.), which could also explain the higher adsorption of EE2 onto RC film due to the molecules' desire to minimize contact with the aqueous environment. Remarkably, adsorption on unmodified RC was three times higher than on chitosan-modified CNF ultrathin film (0.095 nm) and over half of the amount reached for highly engineered cyclodextrin-modified CNF ultrathin film (0.50 nm) (Orelma et al. 2018) indicating the potential of regenerated cellulose materials for water purification purposes. Additionally, EE2 was not significantly desorbed from RC upon rinsing indicating robust attachment (Fig. 1c). The results indicate that nanocellulosic materials may need appropriate surface modification to function as effective filtration materials for hydrophobic pharmaceutical residues.

Pharmaceutical adsorption on hydrophobized cellulose

The effect of surface hydrophobicity on adsorption of ibuprofen, naproxen and 17α-ethinyl estradiol on regenerated cellulose, cellulose triacetate and trimethylsilyl cellulose ultrathin films (surface hydrophobicity RC < CTA < TMSC) was investigated in situ with SPR (Fig. 2). TMSC and CTA are modified cellulose materials with higher hydrophobicity due to the substitution of the hydroxyl groups by trimethylsilyl (DS 2.1–2.3 (Tammelin et al. 2006)) or acetyl groups (DS 2.9), respectively. All tested pharmaceuticals appeared to preferentially adsorb on the



(d)

Surface	Ibuprofen			Naproxen			EE2		
	d (nm)	Γ (mg/m²)	Γ (μmol/m²)	d (nm)	Γ (mg/m²)	Γ (μmol/m²)	d (nm)	Γ (mg/m²)	Γ (μmol/m²)
RC	0.04 ± 0.02	0.04 ± 0.02	0.23 ± 0.09	0.06 ± 0.01	0.07 ± 0.01	0.30 ± 0.03	0.32 ± 0.01	0.38 ± 0.01	1.29 ± 0.03
CNF	0.06 ± 0.01	0.06 ± 0.01	0.28 ± 0.04	0.03 ± 0.01	0.04 ± 0.01	0.17 ± 0.05	0.12 ± 0.00	0.14 ± 0.00	0.48 ± 0.00
TCNF	0.04 ± 0.01	0.04 ± 0.01	0.17 ± 0.04	0.01 ± 0.00	0.02 ± 0.00	0.07 ± 0.02	0.05 ± 0.01	0.06 ± 0.01	0.21 ± 0.03

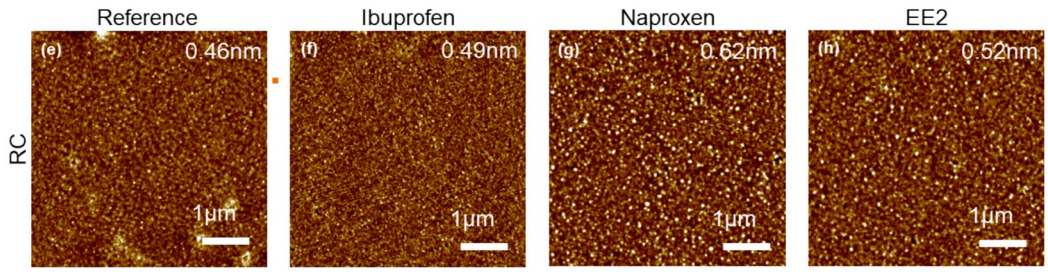
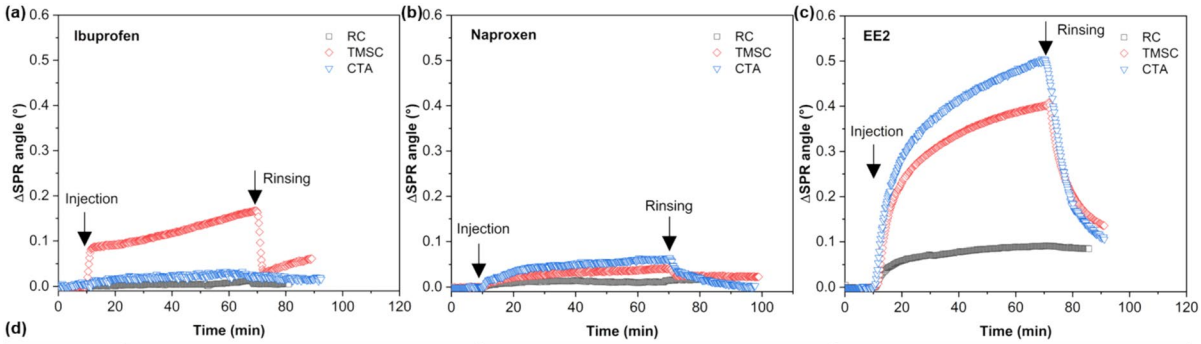


Fig. 1 SPR angle changes upon ibuprofen (a), naproxen (b) and EE2 (c) adsorption (0.1 mg mL^{-1}, 10 mM phosphate buffer, pH 6.8) onto RC (black), CNF (red) and TCNF (blue) films. Arrows indicate substance injections into respective measurement module and rinsing with respective buffer solution. Calculated adsorption layer thicknesses (Eq. 1) and adsorbed amounts (Eq. 2) (d) for the pharmaceuticals. AFM height images (5 × 5 μm^2) of regenerated cellulose surfaces (e) with adsorbed ibuprofen (f), naproxen (g) and EE2 (h) with corresponding rms roughness values included in the upper right corner of image

hydrophobized cellulose surfaces compared to the nanocellulose and regenerated cellulose films based on SPR data (Figs. 1a–c and 2a–c). In case of IBP, adsorption onto CTA (0.08 mg/m^2) was somewhat higher and significantly higher onto TMSC (0.37 mg/m^2) compared to regenerated cellulose (0.04 mg/m^2) (Fig. 2a,d). Notably, IBP adsorption on TMSC also exhibited rapid initial adsorption that leveled fast as opposed to more moderate overall adsorption observed on RC and CTA. However, after rinsing most of the adsorbed IBP was removed from the TMSC film returning to a similar level as for CTA, which was not as significantly rinsed from the surface, indicating somewhat weak interaction of IBP with TMSC. For naproxen, the adsorption was almost negligible on all surfaces with a slightly higher amount indicated for TMSC and CTA than for RC. For cellulose triacetate film, apparently all adsorbed NPR was removed from surface, whereas only about half of adsorbed material was removed from trimethylsilyl cellulose film upon rinsing (Fig. 2b). Rinsing had little effect on naproxen adsorption on RC. The recorded adsorbed amounts for NPR after rinsing were 0.07, 0.10 and 0.08 mg/m^2 for RC, TMSC and CTA surfaces, respectively (Fig. 2d).

Compared to RC film, the estrogenic hormone 17α-ethinyl estradiol adsorption was almost ten times higher on CTA and eight times higher on TMSC,



(d)

Surface	Ibuprofen			Naproxen			EE2		
	d (nm)	Γ (mg/m²)	Γ (μmol/m²)	d (nm)	Γ (mg/m²)	Γ (μmol/m²)	d (nm)	Γ (mg/m²)	Γ (μmol/m²)
RC	0.04 ± 0.02	0.04 ± 0.02	0.23 ± 0.09	0.06 ± 0.01	0.07 ± 0.01	0.30 ± 0.03	0.32 ± 0.01	0.38 ± 0.01	1.29 ± 0.03
TMSC	0.39 ± 0.04	0.37 ± 0.04	1.81 ± 0.18	0.09 ± 0.01	0.10 ± 0.01	0.45 ± 0.03	0.43 ± 0.04	0.52 ± 0.05	1.75 ± 0.16
CTA	0.09 ± 0.05	0.08 ± 0.05	0.40 ± 0.24	0.06 ± 0.05	0.08 ± 0.06	0.33 ± 0.25	0.38 ± 0.04	0.46 ± 0.04	1.56 ± 0.15

Fig. 2 SPR angle changes upon ibuprofen (a), naproxen (b) and EE2 (c) adsorption (0.1 mg mL^{-1}, 10 mM phosphate buffer, pH 6.8) onto RC (black), TMSC (red) and CTA (blue) films. Arrow symbols indicate substance injection into respective measurement module and rinsing with respective buffer solution. Included also respective calculated thicknesses (Eq. 1) and adsorbed amounts (Eq. 2) for IBP, NPR and EE2 onto RC, TMSC and CTA (d)

respectively, prior to rinsing (Fig. 2c). Significantly higher adsorbed amounts for EE2 were observed on all experimented ultrathin films than for ibuprofen or naproxen (Fig. 2). However, upon rinsing, the adsorbed amounts of EE2 on CTA (0.46 mg/m^2) and TMSC (0.52 mg/m^2) reduced closer to the value reached for RC (0.38 mg/m^2), which was not significantly affected by rinsing. Overall, rinsing did not remove the tested pharmaceuticals from the pure regenerated cellulose surfaces whereas desorption of the attached substances from CTA and TMSC surfaces upon rinsing was observed. The adsorption behavior and calculated adsorbed amounts of IBP and NPR are of similar magnitude as for previously reported for non-steroidal anti-inflammatory drugs for different types of surfaces in SPR and QCM-D (~0.5 mg/m^2 and 0.67 mg/m^2 for IBP on gold surface and PDADMAC multilayers, respectively) (Sebők et al. 2013; Yilmaz-Aykut and Deligöz 2023).

Overall, the SPR data suggests that the pharmaceutical adsorption on the cellulosic surfaces was driven by hydrophobic interactions. However, the interactions were not very strong as rinsing decreased the attached amount of material, especially EE2, on the CTA and TMSC ultrathin films reaching ultimately similar levels as for RC films. The reversibility of the adsorption could be caused by the very water-swollen state of the hydrophobized cellulose films where the pharmaceuticals adsorb through hydrophobic interactions, but the coupled water of the cellulose layer prohibits robust attachment resulting in removal of pharmaceuticals with low energy rinsing. The relatively weak interactions may be beneficial in some forms of water purification systems as it implies easy regeneration of material and reduced clogging or fouling of membranes.

AFM height and phase images showed changes for pharmaceutical adsorption on TMSC and CTA films that matched the SPR data (Fig. 3 and Fig. S3). For TMSC films, no significant changes were observed in the height images for any adsorbed pharmaceuticals (Fig. 3a–d) as was somewhat expected due to the small size of pharmaceutical molecules. However, the phase images showed elasticity change of the film surface due to the adsorbed material (Fig. S3a–d). For pharmaceutical adsorption on CTA film, both height and phase images exhibited changes (Fig. 3e–h and Fig. S3e–h). Clusters of adsorbed material were observable on the CTA films for all tested pharmaceuticals, suggesting aggregation of the drugs likely due to their hydrophobic nature and drying of the film after experiment. The clustering was less evident for adsorbed IBP on CTA (Fig. 3f and Fig. S3f) and more pronounced for EE2 (Fig. 3h and Fig. S3h), indicating that the more hydrophobic the pharmaceutical, the more aggregation occurred upon adsorption

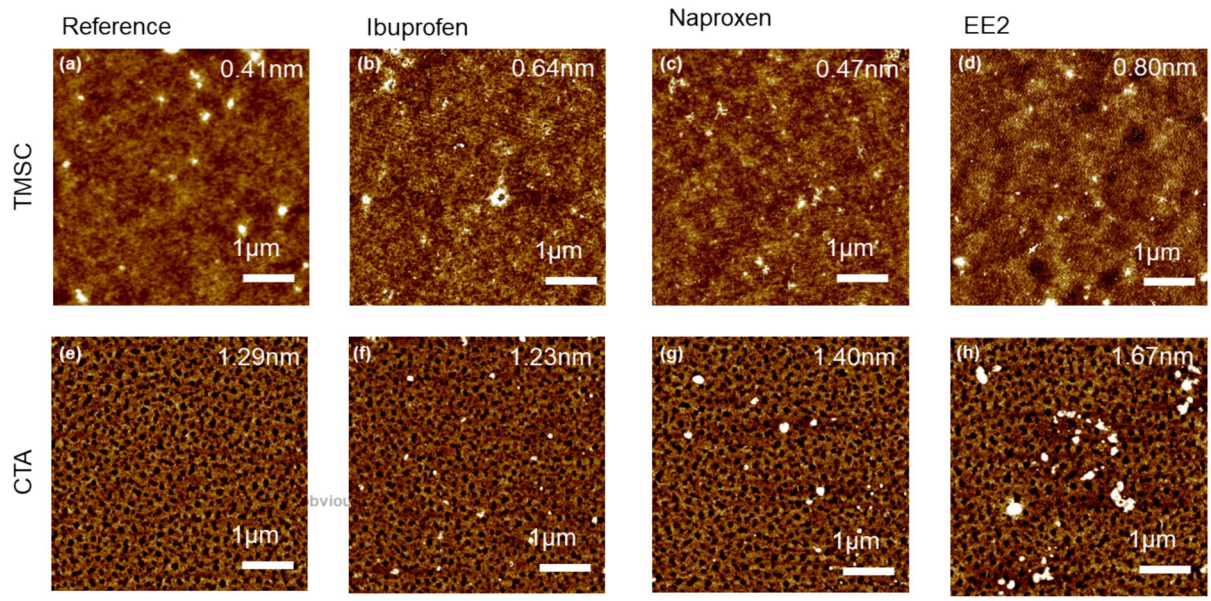


Fig. 3 AFM height images (5×5 μm^2) for TMSC ultrathin films (a) with adsorbed IBP (b), NPR (c) and EE2 (d) and for CTA films (e) with adsorbed IBP (f), NPR (g) and EE2 (h). Included in the upper right corner of height images RMS roughness values for respective films

and film drying. The changes in RMS roughness values (Table S1) for the CTA films supported this conclusion as the values slightly increased for NPR (1.40 nm) and EE2 (1.67 nm) compared to values obtained for reference (1.29 nm) and IBP (1.23 nm). Similarly, as indicated by AFM phase images and SPR data, the RMS roughness values were increased for adsorbed IBP (0.64 nm) and EE2 (0.80 nm) on TMSC surface while the values for adsorbed NPR (0.47 nm) and reference TMSC (0.41 nm) remained similar.

Based on experimental data, the pharmaceuticals, and especially EE2, were adsorbed on the cellulosic films through hydrophobic interactions. The hydrophobized cellulose surfaces had lower affinity for water and higher affinity for the pharmaceuticals, which increased the partitioning of the pharmaceuticals from the aqueous phase to the solid phase. Notably, the calculated adsorbed layer thicknesses for EE2 on trimethylsilyl cellulose and cellulose triacetate (0.43 and 0.38 nm, respectively) were comparable to values obtained for chitosan-modified CNF with conjugated cyclodextrin (0.5 nm) (Orelma et al. 2018) (Table 1) highlighting the removal efficiency of the simple hydrophobized cellulose films compared to highly complex engineered nanocellulose systems. Even on unmodified RC, the calculated layer thickness of adsorbed EE2 (0.32 nm) reached a significantly higher value than on chitosan-modified CNF ultrathin film (0.095 nm) (Orelma et al. 2018) (Table 1). The apparent adsorbed amounts of EE2 on regenerated and hydrophobized cellulose films were also remarkably higher than reported for commercial benchmark activated carbon adsorbents (0.01–0.04 mg/m^2) but lower than those obtained for aliphatic polyamide particles (1.26 mg/m^2)(Han et al. 2013) (Table 1).

The results demonstrate direct evidence that interactions between the cellulosic films and hormonal 17α-ethinyl estradiol could be influenced by modifying surface hydrophobicity. Similarly, as cyclodextrin-modified CNF has been reported to capture EE2 from solution due to its hydrophobic cavity (Orelma et al. 2018), the surface hydrophobization of the cellulose film increased affinity between the materials. A clear trend of higher adsorption of EE2 was achieved with increased surface hydrophobicity based on experimental data (Table 1). The hydrophobized cellulose ultrathin films surpassed the capabilities of benchmark activated carbon absorbents and presented potential to rival synthetic polyamide particles as a more

Table 1 The calculated layer thicknesses (Eq. 1) and adsorbed amounts (Eq. 2) of EE2 on the tested cellulosic ultrathin films with comparison reference material values obtained from literature

Adsorbent material	Adsorbed layer thickness (nm)	Adsorbed amount of EE2 (mq/m^2)
CNF	0.12 ± 0.00	0.14 ± 0.00
TEMPO-CNF	0.05 ± 0.01	0.06 ± 0.01
Regenerated cellulose	0.32 ± 0.01	0.38 ± 0.01
TMSC	0.43 ± 0.04	0.52 ± 0.05
CTA	0.38 ± 0.04	0.46 ± 0.04
Literature values		
Chitosan-modified CNF (Orelma et al. 2018)	0.095	N/A
Cyclodextrin-modified CNF (Orelma et al. 2018)	0.50	N/A
Benchmark activated carbon adsorbents (Han et al. 2013)	N/A	0.01–0.04
Aliphatic polyamide particles (Han et al. 2013)	N/A	1.26

sustainable alternative for water purification purposes in future (Table 1).

Effect of concentration on pharmaceutical adsorption

The effect of concentration on pharmaceutical adsorption on RC, TMSC and CTA was tested by adsorbing IBP, NPR and EE2 with three increasing concentrations of 0.1, 1, 10 and 100 µg/mL consecutively on the surfaces as monitored in real-time by SPR (Fig. S4). The calculated adsorbed amounts (Eqs. 1 and 2) of pharmaceuticals onto pure and hydrophobized cellulose films based on SPR data were fitted to Langmuir adsorption isotherm (Eq. 3) (Fig. 4), which is a monolayer adsorption theory. In case of IBP, the adsorption of lowest concentration was minimal on all the surfaces, but with each increasing concentration higher adsorption was achieved with significantly highest values observed on TMSC (Fig. S4a). The observed adsorption behavior was similar to recorded for IBP on TMSC previously (Fig. 2a), especially in case of the two higher concentrations of 10 and 100 µg/mL with very fast initial adsorption followed by removal of material upon rinsing. After rinsing the calculated adsorbed amounts for IBP were TMSC > CTA > RC (Fig. 4a).

The adsorbed amount of NPR on regenerated cellulose, trimethylsilyl cellulose and cellulose triacetate increased with each increase of concentration similarly as for IBP (Fig. 4b). The highest adsorption prior to rinsing was observed for CTA film, however, after rinsing the highest amount remained on TMSC (Fig. S4b), which was consistent with previous SPR data (Fig. 2b). For estrogen hormone adsorption on RC, TMSC, and CTA (Fig. S4c) with increasing concentration, similar adsorption behavior was observed:

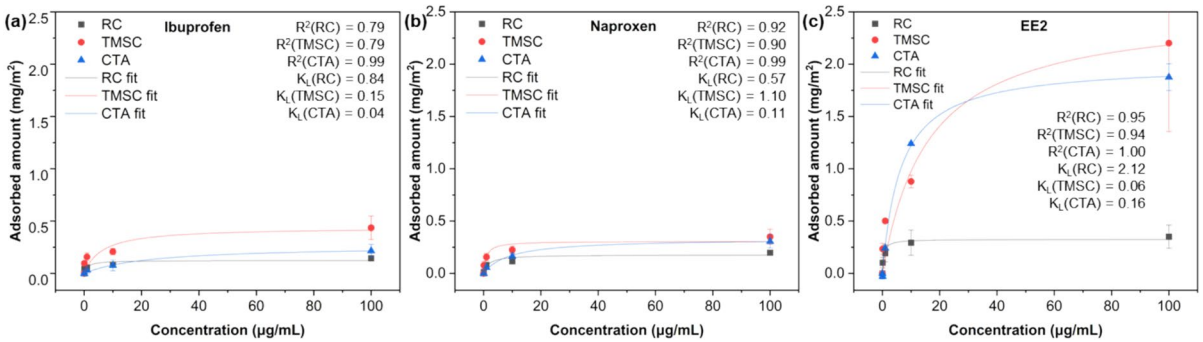


Fig. 4 Fitting of experimental data to Langmuir adsorption isotherm (Eq. 3) for ibuprofen (a), naproxen (b) and EE2 (c) adsorbed on RC (black), TMSC (red) and CTA (blue)

lowest affinity towards regenerated cellulose and almost equal adsorption towards hydrophobized cellulose surfaces prior to rinsing. After rinsing, the adsorption on CTA returned to a similar level than that of RC while the amount on TMSC remained remarkably higher. The adsorption data of EE2 was fitted to Langmuir isotherm at same time of rinsing at 180 min for all three films (Fig. S4c and Fig. 4c). The data confirmed that hydrophobized cellulose materials offer great potential to catch pharmaceutical residues from water samples even at very low concentrations.

Overall, significantly higher adsorption of EE2 to all surfaces, regenerated cellulose, trimethylsilyl cellulose and cellulose triacetate, was observed than for IBP and NPR, which was consistent with previous SPR data (Fig. 2). Furthermore, even very low concentrations of the small hormonal molecule could be observed adsorbing on TMSC (Fig. S4). The higher hydrophobicity of estrogen compared to the other pharmaceuticals based on the octanol–water coefficient and solubility data (p. PubChem Compound Summary for CID 5991, Ethinyl Estradiol., p. PubChem Compound Summary for CID 3672, Ibuprofen., p. PubChem Compound Summary for CID 156391, Naproxen.) resulted in higher affinity for the more hydrophobic surfaces TMSC and CTA as EE2 sought to minimize interaction in aqueous buffer solution. The data implied that even moderate hydrophobic modification of the cellulosic surfaces resulted in significant affinity increase for EE2. For all pharmaceuticals, the highest adsorbed amounts were recorded for TMSC after rinsing, likely due to the most hydrophobic nature of the film (Fig. 4c) resulting in strongest interactions. This can prove to be highly advantageous information for designing sustainable cellulose-based water purification systems.

The calculated (Eqs. 1 and 2) adsorbed amounts of pharmaceuticals on pure regenerated and hydrophobized cellulose films based on SPR data were fitted to Langmuir adsorption isotherm (Eq. 3) (Fig. 4). The obtained R^2 values of fitting the experimental SPR data values for pharmaceutical adsorption on RC, TMSC and CTA (Table S2.) indicated excellent fit for 17α-ethinyl estradiol (R^2 0.94–1.00). In case of naproxen adsorption, the R^2 values for Langmuir adsorption isotherm fitting ranged from 0.90 to 0.99. However, for ibuprofen, even though a good fit was obtained for CTA adsorption data (R^2 0.99), for TMSC and regenerated cellulose films the R^2 values were 0.79 indicating unideal fitting of experimental data.

The fitting of experimental SPR data revealed maximum adsorption capacities q_m for all pharmaceuticals on the respective cellulosic films (Table S2). The lowest adsorption capacity for regenerated cellulose films was obtained for IBP (0.12 mg/m^2) and the highest for EE2 (0.33 mg/m^2). In the case of trimethylsilyl cellulose ultrathin film, the highest capacity was again observed for the estrogenic drug (2.5 mg/m^2) whereas naproxen obtained the lowest value (0.31 mg/m^2). For cellulose triacetate, IBP was found to exhibit lower capacity than for TMSC (0.26 and 0.44 mg/m^2, respectively), possibly due to the somewhat less hydrophobic nature of the CTA film and the more hydrophobic nature of the ibuprofen molecule. For naproxen, similar maximum adsorption capacity values were obtained for both TMSC and CTA (0.31 and 0.33 mg/m^2, respectively), indicating that the slight difference in degree of hydrophobicity of the respective film, did not have significant impact on adsorption capacity. For 17α-ethinyl estradiol, maximum adsorption capacity for CTA (2.0 mg/m^2) was of similar magnitude as for TMSC (2.5 mg/m^2) when values for analysis and fitting were obtained at the same time of rinsing for both. The adsorption data revealed that for trimethylsilyl cellulose film, EE2 could be adsorbed even at very low concentration whereas for cellulose triacetate higher concentration is required. The notably high maximum adsorption capacities recorded for EE2 on TMSC and CTA indicated that the hydrophobized cellulose adsorbents had an abundance of available sites for adsorption and they could hold significant amounts of the hormonal adsorbate at saturation.

The adsorption coefficient is defined as the ratio of the equilibrium concentrations of a solute in the solid and liquid phases, and it reflects the strength of the interaction between the solute and the surface. The higher the adsorption coefficient, the more likely the solute is to be adsorbed on the surface. The adsorption coefficients K_L obtained through fitting the Langmuir isotherm (Table S2) revealed low coefficient values for CTA films (0.04–0.16) for all pharmaceuticals. Fitting experimental data revealed highest K_L values on regenerated cellulose for ibuprofen (0.84) and EE2 (2.1). The highest adsorption coefficient for TMSC film was obtained with NPR (1.1). However, for EE2

the fitted K_L values were low on TMSC (0.06) and CTA (0.16) suggesting that the binding strengths of the hormonal drug to the cellulose adsorbents were relatively weak. Considering that EE2 exhibited the highest maximum adsorption capacities for TSMC and CTA, it could be speculated that while the hydrophobized cellulose films could hold a large amount of hormone, the interaction between them was not very strong. This combination of maximum adsorption capacity and adsorption coefficient suggested that EE2 was easily desorbed from the cellulosic films or that higher concentrations of the pharmaceutical were required to achieve significant adsorption. These implications were in accordance with the experimental SPR data as significant adsorption of EE2 was observed initially due to low solubility of EE2 in water followed by removal of most drug from the TMSC and CTA films upon rinsing. The highest K_L value 2.1 for EE2 adsorbed on RC indicated stronger interactions between the materials, which also correlated well with SPR data (Figs. 1c and 2c) as EE2 was not significantly removed from RC upon. These findings suggested that surface hydrophobicity played a major role in the adsorption process of hormonal drug residues on cellulosic materials as more binding sites became available to the drug while possibly the highly hydrated state of the cellulosic film prevented stronger irreversible interactions. The hydrophobicities of the cellulosic ultrathin films were further investigated with surface free energy determination to further elaborate the role of surface properties on pharmaceutical adsorption.

Contact angle measurements and surface energy of pure regenerated and hydrophobized cellulose ultrathin films

Surface free energy of a surface influences interfacial processes, such as adsorption. To assess the impact of surface energy to the adsorption of pharmaceuticals on pure and hydrophobized cellulosic materials, contact angles with liquids of different surface tension were measured (Fig. 5) and the dispersive acid and base contributions of the surface free energy were calculated based on the acid–base theory (Table S3). The recorded WCA value for RC (37° at 50% RH) correlated well for values reported previously for similar ultrathin films (31° for Langmuir Blodgett deposited regenerated cellulose (Tammelin et al. 2006) and for spin-coated films 47° at ambient conditions and

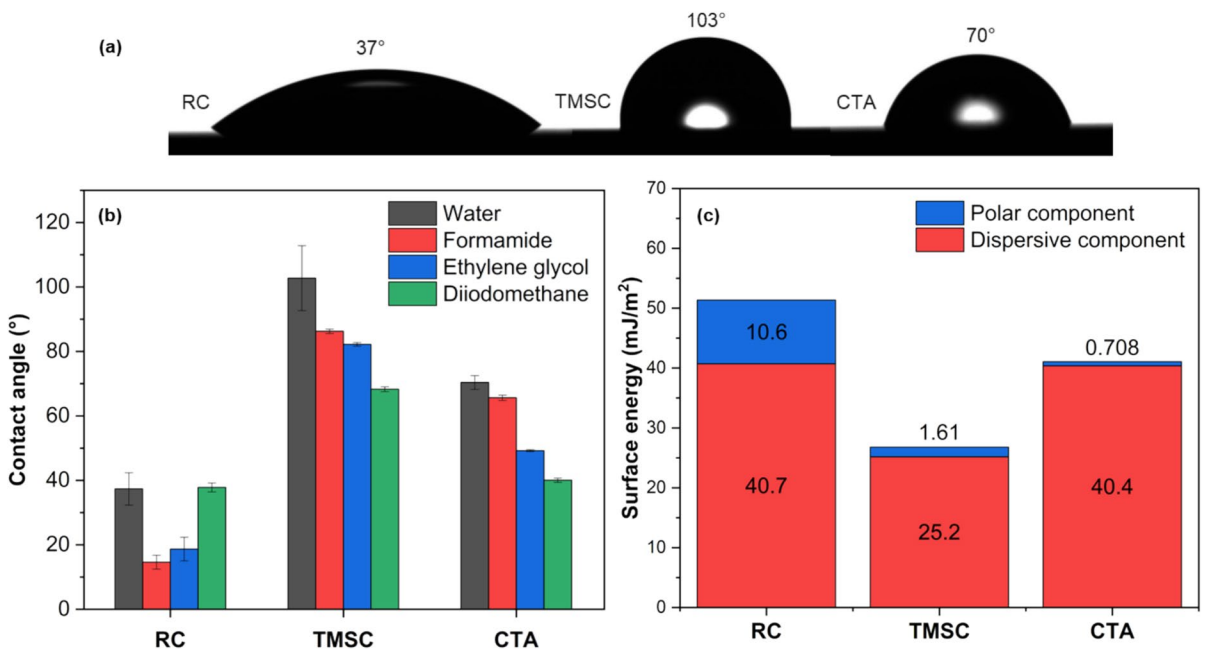


Fig. 5 Water contact angle images (a), contact angle values with four probing liquids (b), and surface free energy with polar and dispersive components(c) for RC, TMSC and CTA films. The standard deviation in the data (c) is less than 5%

27° (after wetting and drying)) (Kontturi et al. 2011). The measured WCA values for TMSC and CTA were 103° and 70°, respectively (Fig. 5a,b), indicating more hydrophobic nature of the films compared to pure regenerated cellulose film due to the silyl and acetyl groups present on the materials. The SE for RC, TMSC and CTA films were determined as 51.3, 26.8 and 41.0 mJ/m^2, respectively. The interactions that operate via dipole, induction, and hydrogen bonding are typically incorporated into the polar or acid–base component of surface free energy. The lower SE values of TMSC and CTA films were composed almost only of the dispersive component (γ^d), while the polar component (γ^p) values were much lower at 1.6 and 0.7 mJ/m^2, respectively, compared to the RC film value of 10.6 mJ/m^2 (Fig. 5c). The γ^p of total SE was even lower for CTA than for TMSC. The SE values obtained for TMSC and CTA were of same order of magnitude as previously reported for similar materials (Mohan et al. 2011; Rbihi et al. 2020).

The results also indicated strong electron-donating nature of the RC film as the electron donor Lewis base component overwhelmingly dominated over the electron-acceptor Lewis acid component ($\gamma^- >> \gamma^+$) signifying the film's ability to participate in polar interactions (Table S3). The electron donor component γ^- was somewhat reduced for the RC film (35 mJ/m^2) compared to the nanocellulose films due to the lack of acidic groups present on its structure. Significantly reduced γ^- values for TMSC and CTA films (3 and 8 mJ/m^2) were associated with the absence of acidic groups on the materials and the presence of silyl and acetyl groups, respectively, the effect being more pronounced for TMSC. The reduced ratio between base and acid components could be indicative of more amphoteric nature of the RC and TMSC surfaces compared to the nanocellulosic ones (Table S3).

The interaction between the molecules of the solid substrate and water, the interfacial free energy ΔG_{sws}^{IFE}, determines the water affinity of the films. The positive ΔG_{sws}^{IFE} values indicate that the polar attraction among water molecules is weaker than the difference between the nonpolar attraction and the polar repulsion when submerged in water. This implies that the material interacts strongly with water and the surface is regarded as hydrophilic. The material surface is considered hydrophobic with negative ΔG_{sws}^{IFE} values as the material immersed in water avoids contact with water and has high cohesive energy. Hence, the sign and magnitude of ΔG_{sws}^{IFE} can indicate the type of surface and the degree of surface hydrophilicity, respectively. The value obtained (Eq. 5) for pure RC films (9 mJ/m^2) was positive indicating hydrophilic character but much lower than for the nanocellulose films (35–39 mJ/m^2) implying lower hydrophilicity of the film from lack of residual hemicellulose and carboxyl groups (Table S3). Negative ΔG_{sws}^{IFE} values were recorded for TMSC < CTA films, indicating their hydrophobic character due to substituted trimethylsilyl and acetyl groups, where TMSC (DS ~ 2.1–2.3) exhibited the lower negative value (−62 mJ/m^2) representing greater degree of hydrophobicity than that of the CTA (43–44% acetyl content, DS ~ 2.9) film (−44 mJ/m^2). Based on the SPR data (Fig. 2d), CA measurements, and SE calculation, the higher adsorption of the pharmaceutical molecules on TMSC and CTA surfaces than on nanocellulosic ones was caused by the higher hydrophobicity of respective ultrathin films. The highest adsorption of all pharmaceuticals was recorded on TMSC (Fig. 2d), which was also the most hydrophobic film. In the case of EE2, the somewhat decreased hydrophilicity of RC film compared to the nanocellulose films was enough to significantly increase adsorption. The decreased hydrophilicity of RC film resulted in very strongly adsorbed EE2 as it was not significantly removed by rinsing as opposed to the TMSC and CTA films (Fig. 2c). The quantified SE by contact angle measurements verified the extent of hydrophobization of the cellulose films TMSC and CTA, which clearly contributed to increased adsorption on more hydrophobic surfaces especially for hormonal pharmaceutical. The surface energy calculations further verified the conclusion that interaction with EE2 could be influenced by modifying the hydrophobicity of the cellulosic surfaces.

Reversibility of the binding of pharmaceuticals on hydrophobized cellulose films

To assess the functionality of cellulosic films as filtration membranes or adsorbent materials, the reversibility of pharmaceutical adsorption on RC and TMSC in SPR was tested with ethanol and sodium dodecyl sulphate (Fig. 6a,b). Ethanol was selected due to excellent solubility of all pharmaceuticals and SDS due to being a common detergent. CTA ultrathin films did not endure the regeneration process on the SPR

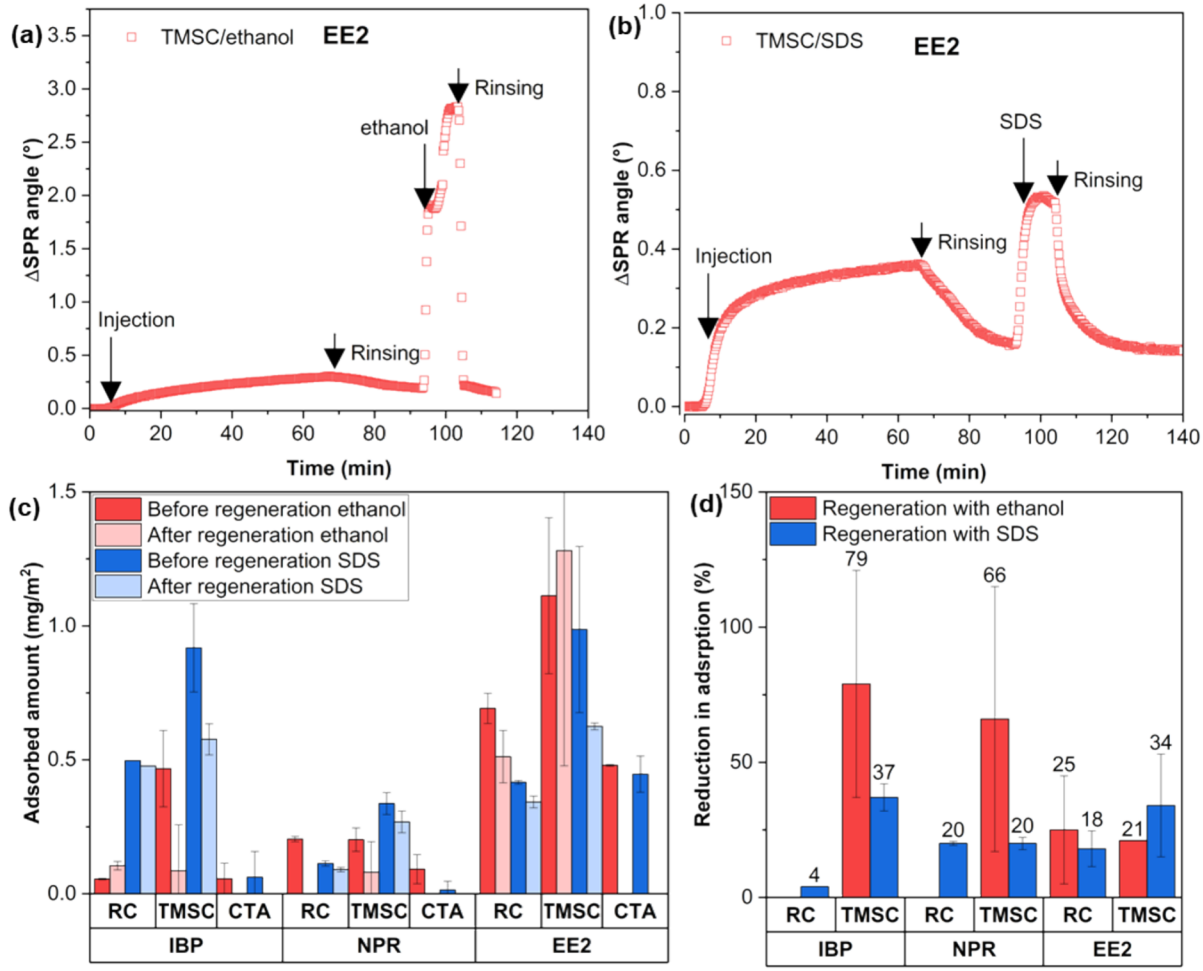


Fig. 6 SPR angle changes upon EE2 adsorption (0.1 mg/mL, 10 mM phosphate buffer, pH 6.8) on TMSC films with ethanol (a) and SDS (b) regeneration. Arrow symbols indicate substance injections into respective measurement module and rinsing with respective buffer solution. Included also a bar chart of calculated adsorbed amounts of pharmaceuticals on pure regenerated and hydrophobized cellulosic films before and after regeneration (c) and calculated removal efficiencies of pharmaceuticals from RC and TMSC films with ethanol and SDS (d)

sensor surface and were, therefore, excluded from the experiments.

The irreversibility of adsorption on RC and TMSC surfaces varied between pharmaceuticals tested with ethanol and SDS. For IBP adsorption on regenerated cellulose, the ethanol treatment caused some rearrangement of the surface and an increase in signal was observed upon regeneration (Fig. 6c). SDS regeneration had minimal effect on RC and did not significantly remove adsorbed IBP. Ibuprofen adsorption on TMSC was found to be somewhat reversible as ethanol regeneration resulted in 79% reduction in adsorbed amount whereas SDS indicated only 37% reduction (Fig. 6c,d). For NPR adsorption onto regenerated and trimethylsilyl cellulose, ethanol regeneration desorbed 66% of said pharmaceutical from TMSC while SDS yielded only 20% removal from both surfaces. Irreversibility of adsorption was somewhat lower for adsorbed 17α-ethinyl estradiol, reaching only 25% and 21% efficiencies for ethanol, and 18% and 34% for SDS on RC and TMSC, respectively, indicating robust attachment of the hormone. Desorption tests revealed that the pharmaceuticals were mainly irreversibly adsorbed on the pure and hydrophobized cellulose surfaces, especially hormonal EE2. Overall, most of the reversibly adsorbed

pharmaceuticals were removed from cellulosic films by rinsing with adsorption media and the remaining adsorbed material was not efficiently desorbed by more robust regeneration of the surface with ethanol and SDS, the latter being somewhat more efficient. Moreover, especially in case of EE2 buffer rinsing on TMSC removed most of loosely adhered material without significant increase obtainable with ethanol or SDS indicating that the remaining EE2 was irreversibly adsorbed though hydrophobic interactions. In case of EE2, adsorption on RC appeared to be mostly irreversible as neither buffer rinsing nor regeneration with ethanol or SDS removed attached material significantly.

Effect of pH on naproxen adsorption on regenerated cellulose film

Naproxen was chosen as model pharmaceutical due to its lowest hydrophobicity according to its octanol–water partition coefficient (p. PubChem Compound Summary for CID 156391, Naproxen.) and as it contains a carboxylic acid group that can be ionized depending on the pH. Substrate selection was based on the least susceptibility to pH variation leading to pure regenerated cellulose with OH groups present on the structure. According to the SPR data (Fig. 7), adsorption of naproxen on RC was elevated at both pHs of 4 (0.2 ± 0.01 mg/m^2) and 9.5 (0.4 ± 0.03 mg/m^2) compared to pH 6.8 (0.07 ± 0.01 mg/m^2). Rinsing removed more NPR from regenerated cellulose at pH 4 than at pH 9.5. The observed increased adsorption at pH 9.5 could be the result of increased polar interactions as the carboxylic acid groups are in a more deprotonated form. At pH 4 the carboxylic acid groups are more protonated possibly resulting in increased hydrophobic interaction between RC and NPR observed as increased adsorption in SPR.

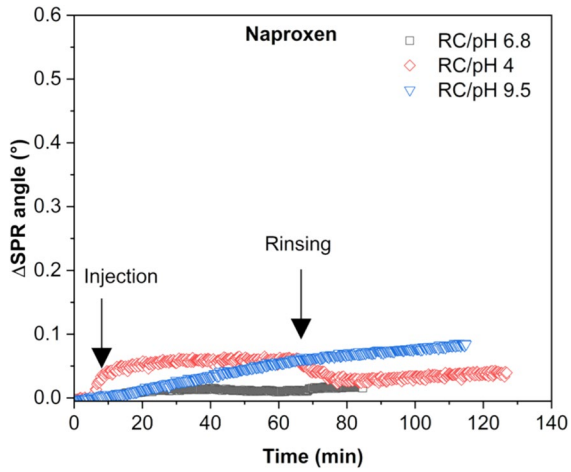


Fig. 7 SPR angle changes upon naproxen adsorption (0.1 mg/mL, 10 mM phosphate buffer, pH 6.8) onto RC at pH 6.8 (black), pH 4 (red) and pH 9.5 (blue). Arrow symbols indicate substance injections into respective measurement module and rinsing with respective buffer solution

Conclusions

Anti-inflammatory and hormonal pharmaceutical interactions with different cellulosic surfaces were examined focusing on parameters such as, surface charge, hydrophobicity, concentration and pH. At neutral pH high charge density did not increase adsorption of any experimental pharmaceutical onto cellulosic material and minimal interactions were observed with CNF and TCNF films according to SPR data and AFM imaging. Higher adsorption of pharmaceuticals was recorded on trimethylsilyl cellulose (TMSC) and cellulose triacetate (CTA) surfaces due to their hydrophobic nature with TMSC demonstrating the highest pharmaceutical adsorption, particularly for hormonal drug EE2 (0.52 mg/m^2). Relevant amount of EE2 was also found to adsorb on regenerated cellulose with minimal impact of rinsing. The hydrophobized cellulose ultrathin films performed comparably to highly engineered cyclodextrin-modified CNF in EE2 removal, highlighting the relevance of fundamentally understanding interfacial interactions of pharmaceutical residues with cellulosic material and their impact on developing feasible larger scale water purification applications.

The concentration gradient experiments and fitting data to the Langmuir adsorption model revealed that even very small concentrations of the pharmaceuticals, especially EE2, could be adsorbed onto TMSC and CTA due to the low solubility of the respective pharmaceuticals in water. Contact angle and surface energy determinations confirmed the more amphoteric nature of the RC film compared to the nanocellulosic films and the hydrophobic nature of the TMSC and CTA films reflecting the conclusion that surface hydrophobization is an effective way to increase adsorption of low-water

soluble pharmaceutical onto cellulosic films. Additionally, most of the reversibly adsorbed pharmaceuticals were removed by buffer rinsing, while the remaining adsorbed material was not efficiently desorbed by more robust regeneration with ethanol and SDS. By modifying the surface properties of cellulosic films to enhance hydrophobic interactions, we have demonstrated a feasible approach to addressing challenges related to utilizing cellulosic materials in advanced filtration applications. The study confirms that tailored surface modifications can lead to better performance in environmental applications, enabling development of green alternatives for filtration membranes. Further studies are needed to reveal optimal modification routes for cellulose films to capture pharmaceutical residues and develop more efficient membrane materials for water purification. The increased understanding of interactions mechanisms between cellulosic materials and pharmaceutical pollutants presented in this work can have long-lasting relevance not only in fundamental understanding of material interactions but in developing efficient and sustainable alternatives for water purification in the future to enable access to clean water for all.

Acknowledgments The work has received funding from Research Council of Finland funding for postdoctoral researcher with the decision number 338572. The work is part of the Research Council of Finland's Flagship Programme (Competence Center for Materials Bioeconomy, FinnCERES). Suvi Arola is acknowledged for assisting in adsorption fitting.

Author contribution All authors contributed to the study conception and design. Material preparation, data collection and analysis were performed by M.V. All authors contributed to methodology selection and interpretation of data. The first draft of the manuscript was written by M.V. whereas H.O. and T.T. revised the previous versions of the manuscript. All authors read and approved the final manuscript.

Funding Open Access funding provided by Technical Research Centre of Finland.

Data availability Data is provided within the manuscript or supplementary information files.

Declarations

Competing Interests The authors declare no competing interests.

Open Access This article is licensed under a Creative Commons Attribution 4.0 International License, which permits use, sharing, adaptation, distribution and reproduction in any medium or format, as long as you give appropriate credit to the original author(s) and the source, provide a link to the Creative Commons licence, and indicate if changes were made. The images or other third party material in this article are included in the article's Creative Commons licence, unless indicated otherwise in a credit line to the material. If material is not included in the article's Creative Commons licence and your intended use is not permitted by statutory regulation or exceeds the permitted use, you will need to obtain permission directly from the copyright holder. To view a copy of this licence, visit http://creativecommons.org/licenses/by/4.0/.

References

Aguilar-Sanchez A, Jalvo B, Mautner A et al (2021) Waterborne nanocellulose coatings for improving the antifouling and antibacterial properties of polyethersulfone membranes. J Membr Sci 620:118842. https://doi.org/10.1016/J.MEMSCI.2020.118842

Ahankari S, George T, Subhedar A, Kar KK (2020) Nanocellulose as a sustainable material for water purification. SPE Polym 1:69–80. https://doi.org/10.1002/pls2.10019

Ahola S, Salmi J, Johansson L et al (2008a) Model films from native cellulose nanofibrils. Preparation, swelling, and surface interactions. Biomacromol 9:1273–1282. https://doi.org/10.1021/bm701317k

Ahola S, Turon X, Österberg M et al (2008b) Enzymatic hydrolysis of native cellulose nanofibrils and other cellulose model films: effect of surface structure. Langmuir 24:11592–11599. https://doi.org/10.1021/la801550j

Campbell CT, Kim G (2007) SPR microscopy and its applications to high-throughput analyses of biomolecular binding events and their kinetics. Biomaterials 28:2380–2392. https://doi.org/10.1016/j.biomaterials.2007.01.047

Chakraborty A, Adhikary S, Bhattacharya S et al (2023) Pharmaceuticals and personal care products as emerging environmental contaminants: prevalence, toxicity, and remedial approaches. ACS Chem Health Saf 30:362–388. https://doi.org/10.1021/acs.chas.3c00071

Chen H, Sharma SK, Sharma PR et al (2019) Arsenic(III) removal by nanostructured dialdehyde cellulose-cysteine microscale and nanoscale fibers. ACS Omega 4:22008–22020. https://doi.org/10.1021/acsomega.9b03078

Chen H, Sharma SK, Sharma PR et al (2021) Nitro-oxidized carboxycellulose nanofibers from moringa plant: effective bioadsorbent for mercury removal. Cellulose 28:8611–8628. https://doi.org/10.1007/s10570-021-04057-5

Cooper GK, Sandberg KR, Hinck JF (1981) Trimethylsilyl cellulose as precursor to regenerated cellulose fiber. J Appl Polym Sci 26:3827–3836

CSID:137720, https://www.chemspider.com/Chemical-Structure.137720.html, (accessed 13:55, Aug 25, 2024)

CSID:3544, https://www.chemspider.com/Chemical-Structure.3544.html, (accessed 13:57, Aug 25, 2024)

CSID:5770, https://www.chemspider.com/Chemical-Structure.5770.html, (accessed 13:59, Aug 25, 2024)

Das R, Lindström T, Sharma PR et al (2022) Nanocellulose for sustainable water purification. Chem Rev 122:8936–9031. https://doi.org/10.1021/acs.chemrev.1c00683

Das S (2017) Micropollutants in Wastewater: Fate and Removal Processes. In: Ray NM (ed). IntechOpen, Rijeka, p Ch. 5

Durairaj V, Wester N, Etula J et al (2019) Multiwalled carbon nanotubes/nanofibrillar cellulose/Nafion composite-modified tetrahedral amorphous carbon electrodes for selective dopamine detection. J Phys Chem C Nanomater Interfaces 123:24826–24836. https://doi.org/10.1021/acs.jpcc.9b05537

Durairaj V, Liljeström T, Wester N et al (2022) Role of nanocellulose in tailoring electroanalytical performance of hybrid nanocellulose/multiwalled carbon nanotube electrodes. Cellulose 29:9217–9233. https://doi.org/10.1007/s10570-022-04836-8

Eniola JO, Kumar R, Barakat MA, Rashid J (2022) A review on conventional and advanced hybrid technologies for pharmaceutical wastewater treatment. J Clean Prod 356:131826. https://doi.org/10.1016/J.JCLEPRO.2022.131826

Eronen P, Laine J, Ruokolainen J, Österberg M (2012) Comparison of multilayer formation between different cellulose nanofibrils and cationic polymers. J Colloid Interface Sci 373:84–93. https://doi.org/10.1016/J.JCIS.2011.09.028

Ganiyu SO, Sable S, Gamal El-Din M (2022) Advanced oxidation processes for the degradation of dissolved organics in produced water: a review of process performance, degradation kinetics and pathway. Chem Eng J 429:132492. https://doi.org/10.1016/J.CEJ.2021.132492

Ge H, Huang H, Xu M, Chen Q (2016) Cellulose/poly(ethylene imine) composites as efficient and reusable adsorbents for heavy metal ions. Cellulose 23:2527–2537. https://doi.org/10.1007/s10570-016-0973-3

Good RJ, Girifalco LA (1960) A theory for estimation of surface and interfacial energies. III. Estimation of surface energies of solids from contact angle data. J Phys Chem 64:561–565. https://doi.org/10.1021/j100834a012

Goswami R, Singh S, Narasimhappa P et al (2024) Nanocellulose: a comprehensive review investigating its potential as an innovative material for water remediation. Int J Biol Macromol 254:127465. https://doi.org/10.1016/J.IJBIOMAC.2023.127465

Greber G, Paschinger O (1981) Silylderivate der cellulose. Papier

Gupta A, Ladino CR, Mekonnen TH (2023) Cationic modification of cellulose as a sustainable and recyclable adsorbent for anionic dyes. Int J Biol Macromol 234:123523. https://doi.org/10.1016/J.IJBIOMAC.2023.123523

Hakalahti M, Salminen A, Seppälä J et al (2015) Effect of interfibrillar PVA bridging on water stability and mechanical properties of TEMPO/NaClO2 oxidized cellulosic nanofibril films. Carbohydr Polym 126:78–82

Hakalahti M, Faustini M, Boissière C et al (2017) Interfacial mechanisms of water vapor sorption into cellulose nanofibril films as revealed by quantitative models. Biomacromol 18:2951–2958. https://doi.org/10.1021/acs.biomac.7b00890

Han J, Qiu W, Cao Z et al (2013) Adsorption of ethinylestradiol (EE2) on polyamide 612: molecular modeling and effects of water chemistry. Water Res 47:2273–2284. https://doi.org/10.1016/J.WATRES.2013.01.046

Hube S, Eskafi M, Hrafnkelsdóttir KF et al (2020) Direct membrane filtration for wastewater treatment and resource recovery: a review. Sci Total Environ 710:136375. https://doi.org/10.1016/J.SCITOTENV.2019.136375

Hurwitz AR, Liu ST (1977) Determination of aqueous solubility and pKa values of estrogens. J Pharm Sci 66:624–627

Iqbal Z, Tanweer MS, Alam M (2022) Recent advances in adsorptive removal of wastewater pollutants by chemically modified metal oxides: a review. J Water Process Eng 46:102641. https://doi.org/10.1016/J.JWPE.2022.102641

Jung LS, Campbell CT, Chinowsky TM et al (1998) Quantitative interpretation of the response of surface plasmon resonance sensors to adsorbed films. Langmuir 14:5636–5648. https://doi.org/10.1021/la971228b

Junter G-A, Lebrun L (2017) Cellulose-based virus-retentive filters: a review. Rev Environ Sci Biotechnol 16:455–489. https://doi.org/10.1007/s11157-017-9434-1

Khadir A, Motamedi M, Negarestani M et al (2020) Preparation of a nano bio-composite based on cellulosic biomass and conducting polymeric nanoparticles for ibuprofen removal: kinetics, isotherms, and energy site distribution. Int J Biol Macromol 162:663–677

Kontturi E, Thüne PC, Niemantsverdriet JW (2003) Cellulose model surfaces—simplified preparation by spin coating and characterization by X-ray photoelectron spectroscopy, infrared spectroscopy, and atomic force microscopy. Langmuir 19:5735–5741. https://doi.org/10.1021/la0340394

Kontturi KS, Tammelin T, Johansson L-S, Stenius P (2008) Adsorption of cationic starch on cellulose studied by QCM-D. Langmuir 24:4743–4749. https://doi.org/10.1021/la703604j

Kontturi E, Suchy M, Penttilä P et al (2011) Amorphous characteristics of an ultrathin cellulose film. Biomacromol 12:770–777. https://doi.org/10.1021/bm101382q

Leppänen I, Lappalainen T, Lohtander T et al (2022) Capturing colloidal nano- and microplastics with plant-based nanocellulose networks. Nat Commun 13:1814. https://doi.org/10.1038/s41467-022-29446-7

Li J, Liu H, Paul Chen J (2018) Microplastics in freshwater systems: a review on occurrence, environmental effects, and methods for microplastics detection. Water Res 137:362–374. https://doi.org/10.1016/j.watres.2017.12.056

Liu S, Zeng J, Tao D, Zhang L (2010) Microfiltration performance of regenerated cellulose membrane prepared at low temperature for wastewater treatment. Cellulose 17:1159–1169. https://doi.org/10.1007/s10570-010-9450-6

Livazovic S, Li Z, Behzad AR et al (2015) Cellulose multilayer membranes manufacture with ionic liquid. J Membr Sci 490:282–293. https://doi.org/10.1016/j.memsci.2015.05.009

Loganathan P, Vigneswaran S, Kandasamy J et al (2023) Treatment trends and combined methods in removing pharmaceuticals and personal care products from wastewater—a review. Membranes (Basel) 13:158. https://doi.org/10.3390/membranes13020158

Ma H, Yoon K, Rong L et al (2010) High-flux thin-film nanofibrous composite ultrafiltration membranes containing cellulose barrier layer. J Mater Chem 20:4692–4704

Ma H, Burger C, Hsiao BS, Chu B (2014) Fabrication and characterization of cellulose nanofiber based thin-film nanofibrous composite membranes. J Memb Sci 454:272–282. https://doi.org/10.1016/j.memsci.2013.11.055

Mansouri F, Chouchene K, Roche N, Ksibi M (2021) Removal of pharmaceuticals from water by adsorption and advanced oxidation processes: state of the art and trends. Appl Sci 11:6659. https://doi.org/10.3390/app11146659

Mautner A (2020) Nanocellulose water treatment membranes and filters: a review. Polym Int 69:741–751

Mestre AS, Pires J, Nogueira JMF, Carvalho AP (2007) Activated carbons for the adsorption of ibuprofen. Carbon 45:1979–1988. https://doi.org/10.1016/j.carbon.2007.06.005

Mohammed N, Grishkewich N, Tam KC (2018) Cellulose nanomaterials: promising sustainable nanomaterials for application in water/wastewater treatment processes. Environ Sci Nano 5:623–658. https://doi.org/10.1039/C7EN01029J

Mohan T, Kargl R, Doliška A et al (2011) Wettability and surface composition of partly and fully regenerated cellulose thin films from trimethylsilyl cellulose. J Colloid Interface Sci 358:604–610. https://doi.org/10.1016/J.JCIS.2011.03.022

Nghiem LD, Manis A, Soldenhoff K, Schäfer AI (2004) Estrogenic hormone removal from wastewater using NF/RO membranes. J Membr Sci 242:37–45. https://doi.org/10.1016/j.memsci.2003.12.034

Orelma H, Virtanen T, Spoljaric S et al (2018) Cyclodextrin-functionalized fiber yarns spun from deep eutectic cellulose solutions for nonspecific hormone capture in aqueous matrices. Biomacromol 19:652–661. https://doi.org/10.1021/acs.biomac.7b01765

Orelma H, Hokkanen A, Leppänen I et al (2020) Optical cellulose fiber made from regenerated cellulose and cellulose acetate for water sensor applications. Cellulose 27:1543–1553. https://doi.org/10.1007/s10570-019-02882-3

Poerio T, Piacentini E, Mazzei R (2019) Membrane processes for microplastic removal. Molecules 24:4148. https://doi.org/10.3390/molecules24224148

Pöhler T, Mautner A, Aguilar-Sanchez A et al (2022) Pilot-scale modification of polyethersulfone membrane with a size and charge selective nanocellulose layer. Sep Purif Technol 285:120341

Qi Y, Guo Y, Liza AA et al (2023) Nanocellulose: a review on preparation routes and applications in functional materials. Cellulose 30:4115–4147. https://doi.org/10.1007/s10570-023-05169-w

Rbihi S, Aboulouard A, Laallam L, Jouaiti A (2020) Contact angle measurements of cellulose based thin film composites: wettability, surface free energy and surface hardness. Surfaces and Interfaces 21:100708. https://doi.org/10.1016/J.SURFIN.2020.100708

Rivera-Utrilla J, Sánchez-Polo M, Gómez-Serrano V et al (2011) Activated carbon modifications to enhance its water treatment applications. An overview. J Hazard Mater 187:1–23. https://doi.org/10.1016/J.JHAZMAT.2011.01.033

Saito T, Nishiyama Y, Putaux J-L et al (2006) Homogeneous suspensions of individualized microfibrils from TEMPO-catalyzed oxidation of native cellulose. Biomacromol 7:1687–1691. https://doi.org/10.1021/bm060154s

Samanta P, Desai AV, Let S, Ghosh SK (2019) Advanced porous materials for sensing, capture and detoxification of organic pollutants toward water remediation. ACS Sustain Chem Eng 7:7456–7478. https://doi.org/10.1021/acssuschemeng.9b00155

SCAN-CM 65:2002 Pulp Total acidic group content – Conductometric titration method, Scandinavian Pulp, Paper and Board Testing Committee

Schäfer AI, Nghiem LD, Waite TD (2002) Removal of the natural hormone estrone from aqueous solutions using nanofiltration and reverse osmosis. Environ Sci Technol 37:182–188. https://doi.org/10.1021/es0102336

Schasfoort RBM, Tudos AJ (2008) Handbook of surface plasmon resonance. Royal Society of Chemistry, Cambridge, UK

Schaub M, Wenz G, Wegner G et al (1993) Ultrathin films of cellulose on silicon wafers. Adv Mater 5:919–922

Sebők D, Csapó E, Preočanin T et al (2013) Adsorption of ibuprofen and dopamine on functionalized gold using surface plasmon resonance spectroscopy at solid-liquid interface. Croat Chem Acta 86:287–295. https://doi.org/10.5562/cca2343

Sharma SK, Sharma PR, Wang L et al (2022) Nitro-oxidized carboxylated cellulose nanofiber based nanopapers and their PEM fuel cell performance. Sustain Energy Fuels 6:3669–3680. https://doi.org/10.1039/D2SE00442A

Siqueira G, Bras J, Dufresne A (2010) Cellulosic bionanocomposites: a review of preparatio, properties and applications. Polymers (Basel) 2:728–765. https://doi.org/10.3390/polym2040728

Solhi L, Guccini V, Heise K et al (2023) Understanding nanocellulose-water interactions: turning a detriment into an asset. Chem Rev 123:1925–2015. https://doi.org/10.1021/acs.chemrev.2c00611

Song W, Lee LY, Ng HY (2020) Chapter 21—Nanofiltration and reverse osmosis processes for the removal of micropollutants. In: Varjani S, Pandey A, Tyagi RD, et al. (eds). Elsevier, pp 527–552

Tammelin T, Saarinen T, Österberg M, Laine J (2006) Preparation of Langmuir/Blodgett-cellulose surfaces by using horizontal dipping procedure. Application for polyelectrolyte adsorption studies performed with QCM-D. Cellulose 13:519–535

Taoufik N, Boumya W, Achak M et al (2021) Comparative overview of advanced oxidation processes and biological approaches for the removal pharmaceuticals. J Environ Manage 288:112404. https://doi.org/10.1016/J.JENVMAN.2021.112404

Tenhunen TM, Peresin MS, Penttilä PA et al (2014) Significance of xylan on the stability and water interactions of cellulosic nanofibrils. React Funct Polym 85:157–166. https://doi.org/10.1016/J.REACTFUNCTPOLYM.2014.08.011

Thomas B, Raj MC, B AK et al (2018) Nanocellulose, a versatile green platform: from biosources to materials and their applications. Chem Rev 118:11575–11625. https://doi.org/10.1021/acs.chemrev.7b00627

Trache D, Tarchoun AF, Derradji M et al (2020) Nanocellulose: from fundamentals to advanced applications. Front Chem 8:392

Van Oss CJ, Chaudhury MK, Good RJ (1988) Interfacial Lifshitz-van der Waals and polar interactions in macroscopic systems. Chem Rev 88:927–941. https://doi.org/10.1021/cr00088a006

Vuoriluoto M, Orelma H, Lundahl M et al (2017) Filaments with affinity binding and wet strength can be achieved by spinning bifunctional cellulose nanofibrils. Biomacromol. https://doi.org/10.1021/acs.biomac.7b00256

AEWiącekKPrzykaza2022Wettability and stability of Naproxen, Ibuprofen and/or Cyclosporine A/silica delivery systemsColloids Interfaces10.3390/colloids6010011Wiącek AE, Przykaza K (2022) Wettability and stability of Naproxen, Ibuprofen and/or Cyclosporine A/silica delivery systems. Colloids Interfaces. https://doi.org/10.3390/colloids6010011

Wong S, Ngadi N, Inuwa IM, Hassan O (2018) Recent advances in applications of activated carbon from biowaste for wastewater treatment: a short review. J Clean Prod 175:361–375. https://doi.org/10.1016/J.JCLEPRO.2017.12.059

Yang Z, Zhou Y, Feng Z et al (2019) A review on reverse osmosis and nanofiltration membranes for water purification. Polymers (Basel) 11:1252. https://doi.org/10.3390/polym11081252

Yilmaz-Aykut D, Deligöz H (2023) Examining layer-by-layer assembly of polyelectrolyte-drug interactions using quartz crystal microbalance with dissipation. Polym Eng Sci 63:3625–3638

Zhang Z, Ahmed AIS, Malik MZ et al (2023) Cellulose/inorganic nanoparticles-based nano-biocomposite for abatement of water and wastewater pollutants. Chemosphere 313:137483. https://doi.org/10.1016/J.CHEMOSPHERE.2022.137483

Publisher's Note Springer Nature remains neutral with regard to jurisdictional claims in published maps and institutional affiliations.